Full Paper

Homoconjugation in Poly(phenylene methylene)s: A Case Study of Non-π-conjugated Polymers with Unexpected Fluorescent Properties

Andreas Braendle,[1] Aleksandr Perevedentsev,[2] Nathan J. Cheetham,[3] Paul N. Stavrinou,[4] Jörg A. Schachner,[5] Nadia C. Mösch-Zanetti,[5] Markus Niederberger,[1] Walter R. Caseri[1]

[1]ETH Zürich, Department of Materials, Multifunctional Materials, Vladimir-Prelog-Weg 5, 8093 Zürich, Switzerland

[2]ETH Zürich, Department of Materials, Polymer Technology, Vladimir-Prelog-Weg 5, 8093 Zürich, Switzerland

[3]Department of Physics and Centre for Plastic Electronics, Imperial College London, London SW7 2AZ, United Kingdom

[4]Department of Engineering Science, University of Oxford, Oxford OX1 3PJ, United Kingdom

[5]Institute of Chemistry, Inorganic Chemistry, University of Graz, Schubertstrasse 1, 8010 Graz, Austria

Correspondence to: Walter R. Caseri (E-mail: walter.caseri@mat.ethz.ch)

Supporting Information is available from the Wiley Online Library or from the author

ABSTRACT

Poly(phenylene methylene) (PPM) exhibits pronounced blue fluorescence in solutions as well as in the solid state despite its non-π-conjugated nature. Optical spectroscopy was used to explore the characteristics and the physical origin of its unexpected optical properties, namely absorption in the 350 nm – 450 nm and photoluminescence in the 400 nm – 600 nm spectral regions. It is shown that PPM possesses two discrete optically-active species, and a relatively long photoluminescence lifetime (>8 ns) in the solid-state. Given the evidence reported herein, π-stacking and aggregation/crystallization, as well as the formation of anthracene-related impurities, are excluded as the probable origins of the optical properties. Instead there is sufficient evidence that PPM supports homoconjugation, that is: π-orbital overlap across adjacent repeat units enabled by particular chain conformation(s), which is confirmed by DFT calculations. Furthermore, poly(2-methylphenylene methylene) and poly(2,4,6-trimethylphenylene methylene) – two derivatives of PPM – were synthesized and found to exhibit comparable spectroscopic properties, confirming the generality of the findings reported for PPM. Cyclic voltammetry measurements revealed the HOMO-LUMO gap to be 3.2 eV – 3.3 eV for all three polymers. The present study illustrates a new approach to the design of light-emitting polymers possessing hitherto unknown optical properties.

KEYWORDS: homoconjugation, poly(phenylene methylene), fluorescence, polymer, spectroscopy

INTRODUCTION

Organic light-emitting polymers typically feature fluorophores that are either (i) incorporated into the polymer backbone, the well-known examples being poly(*p*-phenylene vinylene),[1-3] as well as polyfluorene[4-6] and polythiophene derivatives,[7,8] or (ii) attached to the backbone as a pendant moiety as in the case of poly(2-vinylnaphthalene)[9,10] and poly(9-vinylanthracene).[11,12] In both types, the common feature of the fluorophores is that they consist of a conjugated system of alternating single and multiple covalent bonds over which electrons in (near-)parallel-oriented π-electron orbitals can delocalize. This electronic delocalization lowers the energy gap between the highest occupied (HOMO) and lowest unoccupied (LUMO) molecular orbitals, leading to optical absorption and emission in the wavelength range corresponding to visible light.[13]

Only rarely have non-π-conjugated polymers been reported to be fluorescent; examples include poly(amido amine) (PAMAM) and poly(propylene imine) (PPI) dendrimers which were shown to exhibit blue fluorescence (centered at ~450 nm).[14,15] However, the exact origin of that fluorescence remains unclear.

In addition, unusual fluorescent behavior is not unheard of for compounds in which aromatic units are separated by an electronically 'insulating' alkyl segment such as a methylene group. The classical examples of this are diphenylmethane and its derivatives, for which it was shown that intra-molecular π-orbital overlap could occur across the methylene group, mediated by a near-cofacial arrangement of the two aromatic rings and their close proximity due to the appropriate C–CH_2–C bending angle.[16] Such electronic interaction has been termed '*homoconjugation*' (IUPAC).[17,18] As shown for diphenylmethane derivatives, homoconjugation and the resulting increased electronic delocalization may lead to the expected red-shift in absorption and fluorescence spectra.[19]

Interestingly, it was mentioned that poly(phenylene methylene) (PPM; see **Figure 1**) – in essence, a macromolecular equivalent of diphenylmethane – exhibits fluorescence despite its expected non-π-conjugated nature based on the chemical structure.[20-22] However, to date, fluorescence has been

reported only for PPM solutions, and no detailed spectroscopic studies were undertaken. The understanding of fluorescence dependence on molar mass of the polymer, as well as any information on its solid-state properties, is still lacking. More importantly, however, the exact origin of the unexpected fluorescent properties of PPM has not been explored in sufficient detail. To date its fluorescence has been proposed (but not confirmed) to arise from substituted anthracene units formed as an oxidation product of a side reaction,[20] while the possibility of homoconjugation has not been considered.

PPM was first reported in 1853 by Cannizzaro[23] and is commonly synthesized using benzyl chloride and tin(IV) chloride,[24,25] aluminum(III) chloride[26,27] or iron(III) chloride[22,28] as catalysts. The polymers predominantly comprise para-substituted phenylene rings although ortho- and meta- substitution can also occur.[26,29-31] The molar masses of the products reported to date were typically in the range of 2'000–6'000 g mol^{-1}. In addition to benzyl chloride, benzyl alcohol and aryl methanol derivatives were used as monomers together with tungsten oxide, [32] tungsten(VI) chloride [33] or iron(III) chloride [34] as catalysts.

Here we report an improved synthesis of PPM for yielding material of higher molar mass and present an extensive spectroscopic study aimed at exploring the characteristics and origin of the unusual fluorescent properties of this non-π-conjugated polymer. Furthermore, we synthesized and studied two PPM derivatives – namely, poly(2-methyl phenylenemethylene) (PMPM) and poly(2,4,6-trimethyl phenylenemethylene) (PTMPM) (see Figure 1) – in order to explore the generality of the optical properties of PPM.

RESULTS

Synthesis, structural characterization, and thermal, optical and electrochemical properties

Synthesis and structural characterization

Poly(phenylene methylene) (PPM) was synthesized by polymerization of benzyl chloride with tin(IV) chloride as a catalyst (**Scheme 1**). Unlike in the polymerization reactions reported previously, the reactions were performed *without* solvent at temperatures in the 80 °C – 120 °C range and under a steady nitrogen flow to remove HCl which evolves during polymerization. Due to the increasing viscosity of the reaction mixture over the course of polymerization, a mechanical stirrer was used. Synthesis of PMPM and PTMPM was carried out using a similar procedure (see *Experimental*). Chemical structures and appearance (under white- and UV-light illumination) of PPM and its derivatives are shown in Figure 1, and their respective structural, thermal and electrochemical properties are summarized in **Table 1** and discussed below.

^{1}H-NMR spectra of PPM, PMPM and PTMPM (cf. Figure S1(a-c) in the Supporting Information) show the typical aromatic resonances in the region of 6.8 ppm – 7.2 ppm and the bridging methylene signal at 3.9 ppm, which differs from the corresponding position for the monomer (4.5 ppm). These findings are in agreement with the reported values for PPM.[21,35] In the spectra for PMPM and PTMPM the signals of the methyl substituents arise at 1.9 ppm – 2.4 ppm. The substitution pattern of the polymers could not be determined due to broadening of the signals, which is common for ^{1}H-NMR spectra of polymers. The number-average molar mass (M_n) for all polymers ranged from 5'000 g mol^{-1} to 11'000 g mol^{-1} in a monomodal distribution, with polydispersity indices (PDI = $M_\mathrm{w}/M_\mathrm{n}$) ranging from 3.3 to 6.1 (see Table 1 and Figure S2 in the Supporting Information).

Thermal analysis

Thermogravimetric analysis of the polymers carried out under ambient atmosphere reveals an onset of thermal decomposition between 450 °C and 490 °C while maximum decomposition rates are observed at 509 °C, 511 °C and 482 °C for PPM, PMPM and PTMPM, respectively (cf. Figure S3(a) in the Supporting Information). These values are in agreement with those reported elsewhere.[21,36] Furthermore, close agreement (within 2%) is found for the decomposition onset temperatures determined under air and nitrogen atmospheres.

Differential scanning calorimetry (DSC) performed on neat polymers shows, in each case, only a single glass transition (cf. Figure S3(b) in the Supporting Information). The glass transition temperature (T_g) of the polymers increases with the number of methyl substituents on the phenylene unit. The unsubstituted PPM polymer features $T_g \approx 66$ °C, while the methyl-substituted PMPM and the trimethyl-substituted PTMPM polymers exhibit T_g values of 93 °C and 147 °C, respectively. This is likely due to the relative differences in mobility of the polymer chains, the motion of which is progressively restricted with the increase in the number of methyl substituents, leading to the corresponding increase in T_g.

The lack of any thermal transitions beyond the glass transition temperature indicates that the synthesized PPM polymer and its derivatives are amorphous. While for certain polymers the addition of solvent and the corresponding enhancement in chain mobility may allow crystallization to occur,[6] DSC thermograms recorded for PPM solutions in decahydronaphthalene ('decalin'; a moderately good solvent) are also found to be featureless (data not shown). The lack of crystalline order formation in PPM was further confirmed using temperature-dependent wide-angle X-ray diffraction (see Figure S4 in the Supporting Information), and cross-polarized optical micrographs of spin-coated PPM films did not reveal any birefringence either (data not shown).

Cyclic voltammetry

Cyclic voltammetry (CV) is an established method for estimating the energy levels of an organic polymer.[37] The onset oxidation potential ($E_{ox,onset}$) corresponds to the energy of the HOMO and the onset reduction potential ($E_{red,onset}$) to the energy of the LUMO. $E_{ox,onset}$ and $E_{red,onset}$ for PPM, PMPM and PTMPM are +1.0 V and –2.3 V (PPM) and –2.2 V (PMPM, PTMPM), respectively (Figure S5 in the Supporting Information). The onset oxidation potential of 1.0 V for PPM and its derivatives is considerably lower than that for related small aromatic molecules such as *p*-xylene (1.6 V)[38] or diphenylmethane (1.8 V).[39] The energy levels of the HOMO (E_{HOMO}) and the LUMO (E_{LUMO}) for all polymers were calculated to be at –5.8 eV and –2.6 eV $\pm$ 0.1 eV, respectively (see Table 1). The resulting

HOMO-LUMO gap (ΔE) of ~3.3 eV for PPM and ~3.2 eV for PMPM and PTMPM corresponds to an onset of optical absorption around 375 nm – 390 nm (for comparison, absorption onset of *p*-xylene is ~280 nm[40]).

Optical spectroscopy

PPM solutions

Intra-chain excitations and two-phase structure of absorption and emission spectra

The absorption spectrum of PPM in a semi-dilute solution in chloroform (83 mmol L^{-1} ≈ 0.5% m/m) is shown in **Figure 2**(a) (black line). A vibronically-resolved absorption band is observed between 350 nm and 450 nm with a peak at 385 nm. This absorption band is considerably red-shifted from the expected position of localized (*L*-*L**) transitions for a single phenylene ring (~230–275 nm),[40] the onset of which is seen here at 315 nm. Hence, we assign the absorption band centered at ~385 nm to a *D*1-*D*1* transition, for which both ground and excited states are *delocalized* over several aromatic rings. This excited state of PPM is found to undergo radiative decay, with the corresponding photoluminescence (PL) emission spectrum shown in Figure 2(b) (black line). Thus, given the relatively small Stokes shift (discussed in more detail below) between the absorption and PL spectra, we conclude that PPM supports the formation of *intra-chain singlet excitons*, with the corresponding absorption band centered at ~385 nm hence attributed to the S_0-S_1 HOMO-LUMO transition, which is also broadly consistent with the results of CV measurements.

In order to correlate the recorded PL spectrum (Figure 2(b), black line) with the distinct features of the corresponding absorption spectrum, photoluminescence excitation (PLE) spectroscopy was performed on the same PPM solution. Specifically, PLE spectra were recorded with PL detection at wavelengths corresponding to (i) the *maximum* of the PL spectrum at 445 nm and (ii) the *long-wavelength tail* of the PL spectrum at 550 nm.

The PLE spectrum acquired with detection at 445 nm (Figure 2(a), blue line) features three distinct peaks at 366 nm, 385 nm and 406 nm, as well as a shoulder at 348 nm. Although the onset at 302 nm appears at a slightly reduced wavelength compared with that observed in the absorption spectrum, given its spectral position it is nevertheless assigned to the excitation of the phenylene ring itself. The overall shape and peak positions of the PLE spectrum closely match those of the absorption spectrum below 415 nm; notably, however, the absorption features at wavelengths greater than 415 nm were *not* revealed in the PLE spectrum acquired with detection at 445 nm. By contrast, the PLE spectrum acquired with detection at 550 nm (Figure 2(a), green line) is found to reproduce all the features of the absorption spectrum. Of note are the matching wavelengths of the onset of localized transitions (315 nm) and an increased relative intensity of the high-wavelength spectral features – the latter signifying the occurrence of excitation energy transfer prior to emission (discussed in more detail below).

The observation that different parts of the 'total PL' spectrum (black line in Figure 2(b)) originate from different subsets of absorption features provides compelling evidence for the presence of two optically-active species. The *higher*-energy species is characterized by absorption peaks in 350 nm – 410 nm spectral region. The *lower*-energy species features its absorption maximum at 452 nm and a secondary peak at 428 nm, both of which are appreciably broader than the absorption peaks of the *higher*-energy species, thereby further corroborating the difference between them. Given its distinct, red-shifted absorption, the PL spectrum of the *lower*-energy species can be obtained by site-selective excitation at 438 nm and is shown in Figure 2(b) (solid green line), featuring peaks at 477 nm and 502 nm.

Hereafter, for the sake of simplicity the *higher*- and *lower*-energy optically-active species identified in Figure 2 (i.e. absorption maxima at ~385 and ~452 nm) will be referred to as the *blue*- and *green*-phase, respectively. Such denotation was chosen with reference to the color equivalent of the mean, intensity-weighted PL emission wavelengths of the spectrally-subtracted (vide infra) higher- and lower-energy species (~448 nm and ~500 nm respectively). We note that similar nomenclature has been used

previously in the context of conjugated polymers to distinguish two discrete optically-active species.[41,42]

There are two further nuances to be noted pertaining to the interplay between the two phases. First, while photoexcitation at 388 nm is expected to lead to absorption by (predominantly) the *blue*-phase, the resulting PL spectrum clearly comprises a superposition of both *blue*-phase and *green*-phase emission spectra (Figure 2(b), black line). Second, the PLE spectrum recorded with detection at 550 nm (i.e. predominantly *green*-phase emission) similarly features a substantial contribution from the *blue*-phase (that is, peaks in the 350 nm – 415 nm wavelength range; cf. Figure 2(a)). Taken together, these observations suggest that significant excitation energy transfer occurs from the higher-energy *blue*-phase to the lower-energy *green*-phase within the excitations' radiative lifetime which, reassuringly, was found by our preliminary measurements to be substantially longer (>8 ns in the solid-state; vide infra) than for other blue-emitting conjugated polymers.

As a consequence, the PL spectrum of the *blue*-phase can only be obtained by spectral subtraction, that is: normalization by the long-wavelength tail and subtracting the *green*-phase PL spectrum (recorded with site-selective excitation at 438 nm; dotted green line in Figure 2(b)) from the overall PL spectrum obtained with excitation at 388 nm. The resulting *blue*-phase PL spectrum is shown by the dashed blue line in Figure 2(b). The Stokes shift for both phases was calculated from the difference between the corresponding positions of the 0-0 absorption and PL peak maxima. The values for the *blue*- (17 nm ≈ 123 meV) and *green*-phase (25 nm ≈ 144 meV) are comparable to those typically found for conjugated polymers, e.g. 24 nm ≈ 184 meV for poly(9,9-dioctylfluorene) in solutions in decalin,[6] and indicate that there is a non-negligible degree of conformation rearrangement occurring between the ground and excited states of PPM. At present we do not have a reliable explanation for the origin of the difference between the *blue*- and the *green*-phases of PPM, although it is likely to be related to different electronic delocalization for the respective ground or excited states arising from, for instance, conformational or structural (e.g. combination of ortho-, meta- and para-substitution patterns)

heterogeneities. Determining the origins and the relationship between the two phases will be explored in subsequent studies.

Finally, it is interesting to note that both absorption and PL spectra of PPM exhibit well-resolved vibronic features. Such remarkably well-defined vibronic structure in absorption and PL emission spectra is typically only observed for conjugated polymer systems which meet at least one of the following criteria: They

(i) feature an inherently *rigid* conjugated backbone, e.g. the so-called 'ladder-type' methyl-substituted poly-*p*-phenylene (MeLPPP);[43,44]

(ii) are highly crystalline, as commonly observed for, e.g., poly(3-hexylthiophene) (P3HT);[45]

(iii) feature a certain fraction of chain segments in a precisely defined chain conformation, with the well-known example being the so-called 'β-phase' of poly(9,9-dioctylfluorene).[5,46]

Clearly, the first two possibilities cannot apply to PPM given that its backbone structure is flexible (cf. Figure 1(a)) and, as noted above, thermal analysis did not indicate the occurrence of crystallization from the melt or solutions. The third possibility cannot be ruled out at this stage. The origin of the unusual optical properties of PPM will be explored in subsequent sections of the manuscript.

Degree-of-polymerization dependence

A series of PPM samples possessing degrees of polymerization (DP) ranging from 5 to 110 were synthesized (see *Experimental*) and studied by photoluminescence spectroscopy in solutions in chloroform (~40 mmol L^{-1}). Note that in all cases DP represents an *average* value due to the unavoidable polydispersity of polymer samples.

PL spectra recorded with excitation at 388 nm (not shown) were fitted with a sum of Gaussian functions, each representing a vibronic peak, in order to determine the variation of S_1-S_0 transition energies with DP. The results, presented in **Figure 3**, show that the PL wavelengths, λ_{PL}, corresponding to the *blue*-phase 0-1 and *green*-phase 0-0 vibronic peaks red-shift by up to 6 nm with increasing DP, both reaching

a plateau at DP ≥ 10 monomer units. Such spectral changes are strongly indicative of the electronic delocalization along the chain increasing with molar mass[47] and, therefore, confirm that photoexcitations in PPM in the 350 nm – 450 nm spectral region are *intra*-chain, rather than originating from any *inter*-chain aggregation-induced effects.

We note that similar analysis performed on PLE spectra (detection at 440 nm; data not shown) acquired for the same set of solutions gratifyingly yielded a comparable ~5 nm red-shift for tracking the S_0-S_1 *blue*-phase 0-0 vibronic peak as a function of DP and is therefore fully consistent.

Temperature dependence

To further rule out the possibility of the optical properties of PPM originating from any aggregation-induced effects and to explore the relative stability of the identified phases, temperature-dependent optical spectroscopy was performed on PPM solutions in toluene (289 mmol L^{-1} ≈ 2.9% m/m). The chosen temperature range (10 °C to 90 °C) corresponds to temperatures well-below and well-above the T_g of *neat* PPM (cf. Table 1).

Figure 4 presents the absorption spectra, as well as PL spectra excited at 388 nm (predominantly *blue*-phase excitation) and 438 nm (*green*-phase excitation) acquired at different temperatures. No distinct spectral shifts are observed for any of the spectra, with both absorption and PL stable up to the highest temperature, thereby confirming that the optical properties are unlikely to originate from any inter-chain aggregation effects.

Since the measurements were not carried out in an integrating sphere, it is not possible to comment upon any temperature-dependent changes in the absolute PL quantum efficiency since the observed minor decrease in absorbance and PL intensity with increasing temperature could be related to instrumental factors.

In order to explore the *relative* differences in stability of the two phases as a function of temperature, the *blue*- to *green*-phase absorbance and PL intensity ratios were calculated and are shown in the inset

of Figure 4(b) normalized by the respective values at 10 °C. The absorbance ratio, r_{A}, for a given temperature was calculated by dividing the absorbance recorded at 385 nm by the corresponding value at 452 nm. The PL intensity ratio, r_{PL}, was calculated for the *'total* PL' spectrum (cf. Figure 4(b)) from the ratio of the integrated areas of the constituent *blue*-phase and *green*-phase PL components (as described earlier).

As shown in the inset of Figure 4(b), r_{A} remains virtually constant (within 2%) over the entire temperature range indicating comparable stability for the two phases. On the other hand, r_{PL} increases by >25% upon heating the solutions from 10 °C to 90 °C. Taken together, this suggests that excitation energy transfer from *blue*- to *green*-phase upon excitation at 388 nm is inhibited with increasing temperature, thereby leading to the diminishing *green*-phase contribution to the 'total PL' spectra shown in Figure 4(b). Excitation energy transfer phenomena in PPM will be investigated in subsequent work.

PPM films

The optical properties of PPM in solution – namely, absorption in the 350 nm – 450 nm and photoluminescence in the 400 nm – 600 nm spectral regions – are also present in glassy (i.e. in-plane isotropic) spin-coated films. Specifically, we found that PLE and PL spectra recorded for glassy PPM thin films (thickness ≈ 330 nm; see Figure S6 in the Supporting Information) using comparable detection and excitation wavelengths closely match the corresponding spectra recorded for PPM solutions (cf. Figure 2), including the presence of *blue*- and *green*-phase spectral components.

Absorption spectra for glassy PPM films were recorded in the 350 nm – 450 nm spectral region. For this purpose, relatively thick (~17 μm) PPM films were fabricated by spin-coating from highly concentrated solutions. Absorption spectra of PPM in solution and solid-state film are virtually identical in terms of vibronic resolution and spectral positions of the corresponding peaks, as well as the relative fraction of green-phase absorption at ~452 nm (see Figure S7 in the Supporting Information). This observation is at odds with the majority of π-conjugated polymers,[48] for which

chain extension/planarization and densified packing in the solid-state typically lead to a substantial absorption red-shift. The absorption coefficient (α) measured for PPM thick films at the maximum of *blue*-phase absorption (~386 nm) was determined to be ~0.008×10^4 cm^{-1} (see Figure S8 in the Supporting Information). This value is ~2600 times smaller than the peak absorption coefficient of polydioctylfluorene (PFO)[3] – a prototypical blue-emitting conjugated polymer – and is likely to signify that PPM features a low fraction of chromophores or a low oscillator strength for the corresponding transition.

The latter hypothesis is supported by the results of PL lifetime analysis performed on PPM thin films (as above) which yielded a monoexponential PL decay lifetime τ = 8.55 ns (cf. **Table 2** and Figure S9 in the Supporting Information), which is substantially longer than for excitonic fluorescence of other blue-emitting conjugated polymers. For instance, solid-state PFO exhibits a PL lifetime of only ~250 ps.[49] We note, however, that relatively long fluorescence lifetimes have also been reported for low-density trap states[50,51] owing to the isolated nature of the excitations, which may also be a contributing factor in solid-state PPM given its low absorption coefficient. Subsequent studies will be needed to explore this further.

Photoluminescence quantum efficiency (PLQE) analysis was performed on PPM films (~17 μm thickness) and, for comparison, solutions in chloroform (165 mmol L^{-1}), with the results presented in Table 2. As expected, PLQE value for PPM in solution (69%) is higher than that for solid-state PPM (41%), with the latter value comparable to those typically reported for the high-performance blue-emitting conjugated polymers such as PFO.[46]

Pending further optimization and study, the solid-state optical properties of PPM reported above make it a promising candidate for optoelectronic applications. For instance, its long PL lifetime could allow PPM to be used as an exciton 'reservoir'[52] for continuous feeding of the excited state manifold of a suitably chosen acceptor, while its moderately high PLQE is advantageous for applications in light-emitting devices.

PPM derivatives: PMPM and PTMPM

To establish the generality of the optical properties of PPM, UV-Vis and PL spectroscopy were also performed on solutions of its methyl-substituted derivatives PMPM and PTMPM (cf. Figure 1) in chloroform. As shown in **Figure 5**(a), absorption spectra of PMPM and PTMPM exhibit a minor blue-shift (7 nm and 3 nm, respectively) relative to that of PPM, although all spectra feature similarly well-resolved vibronic structure. Interestingly, however, the characteristic absorption band of the *green*-phase of PPM centered at ~452 nm is not observed for either of its derivatives, suggesting that it may be related to a particular combination of substitution patterns that is absent for PMPM and PTMPM. The trend in the molar extinction coefficient, ε, for the three polymers in solution ($\varepsilon_{\mathrm{PMPM}} < \varepsilon_{\mathrm{PPM}} < \varepsilon_{\mathrm{PTMPM}}$; cf. Figure 5(a)) is consistent with that for their solid-state absorption coefficients, α, determined for ~17 μm-thick spin-coated films (see Figure S8 in the Supporting Information).

PL spectra of the PMPM and PTMPM, as well as PPM for comparison purposes, in chloroform solutions are shown in Figure 5(b). The overall vibronic structure is found to be remarkably similar for all three polymers. The PL spectra of PMPM and PTMPM are blue-shifted by ~10 nm and ~5 nm relative to the PL spectrum of PPM, which is consistent with the trends observed for the main absorption edges in Figure 5(a). Significantly, however, the observation that PPM and its methyl-substituted derivatives exhibit closely-matching absorption and PL spectra (in solutions and solid-state – see Figure 1 and Figure S8 in the Supporting Information) strongly indicates that the optical properties are indeed enabled by the common phenylene-methylene sequence of these polymers.

DISCUSSION

The possible origins of the unexpected optical properties of PPM – namely, absorption in the 350 nm – 450 nm and photoluminescence in the 400 nm – 600 nm spectral regions – will be critically examined below.

Intermolecular interactions

It is well known that aromatic molecules can assemble via interactions of π-electrons ('π-stacking'), whereby aromatic rings adopt a closely-packed arrangement. A frequent consequence of π-π interaction is the formation of excimers upon photoexcitation.[53] Excimers typically have several signature characteristics: first, the absence of any associated ground-state absorption features; second, a large Stokes shift between fluorescence and the absorption spectrum of a single chromophore and, third, the absence of vibronic structure in the corresponding fluorescence spectra.[13,54–57] However, it is clear that none of these apply to PPM since optical spectroscopy indicates that the PL spectra of its *blue*- and *green*-phases are correlated with the respective absorption spectra, featuring small Stokes shifts and well-resolved vibronic structure, thereby confirming the *excitonic* origin its fluorescence.

The optical properties of organic (macro)molecules can also strongly depend on the state of aggregation mediated by π-stacking.[9,58,59] For instance, fluorescence for most small-molecular aromatic hydrocarbon compounds in solution is quenched with increasing concentration, with the quenching typically attributed to the formation of aggregates.[58,60,61] On the other hand, aggregation can also lead to enhancement of fluorescence, for instance due to restriction of intramolecular motion (vibration or rotation)[58,62,63] or J-aggregate formation.[64] In the case of PPM, however, fluorescence was observed both in highly dilute and concentrated solutions, as well as in the solid state.

We therefore exclude π-π stacking – or aggregation mediated thereby – as the origin of the optical properties of PPM. This conclusion is further corroborated by the results of thermal and X-ray diffraction analysis (no order formation for either solutions or solids) and temperature-dependent optical spectroscopy (no spectral shifts over the investigated temperature range).

Formation of 9,10-diphenylanthracene in a side reaction

As mentioned above, previous reports have attributed the fluorescent properties of PPM to 9,10-diphenylanthracene, which was proposed to form in a potential side reaction (**Scheme 2**).[20] This reaction, however, can only proceed if the following prerequisites are fulfilled: A) the presence of phenylene units ortho-substituted with two benzyl groups I for six-membered ring cyclization; B)

elimination of a hydride at the methylene position in the transformation from intermediate I to II, and C) the presence of oxygen to oxidize the dihydroanthracene derivative III to the anthracene derivative IV. Prerequisite A) (i.e. formation of a ortho-substituted dibenzyl product analogous to I) was prevented when 2,4,6-trimethylbenzyl chloride (2,4,6-TMBC) was polymerized into PTMPM, since the meta-positions are blocked by methyl groups. Therefore, no side-reaction resulting in an anthracene derivative could have occurred. Nevertheless, the obtained polymer exhibits fluorescence with spectral characteristics matching those of PPM. B) is considered to be unlikely under the synthetic conditions used, since drastically different conditions are usually required for hydride elimination.[65,66] Regarding C), we observed on the contrary that the presence of oxygen during polymerization *inhibits* fluorescence: the more rigorously oxygen was excluded during the reaction, the more intensely fluorescent was the obtained polymer.

Furthermore, using the reported value for its molar extinction coefficient (~14'000 M^{-1} cm^{-1} at ~372 nm)[67] the potential 9,10-diphenylanthracene concentration can be estimated from the optical absorption spectra recorded for PPM solutions of known concentration. Accordingly, the potential concentration of 9,10-diphenylanthracene in PPM would amount to 0.025% mol/mol, if the 9,10-diphenylanthracene impurity was responsible for the observed absorption spectra of the material. Such concentrations of 9,10-diphenylanthracene in PPM are well above the detection limit of ^{1}H-NMR spectroscopy (as demonstrated in Figure S10 in the Supporting Information) and therefore the presence of 9,10-diphenylanthracene would emerge as a distinct pattern superimposed onto that of PPM. However, the signals associated with 9,10-diphenylanthracene were wholly absent in the ^{1}H-NMR spectrum of PPM.

We also note that cyclic voltammetry did not show comparable behavior for 9,10-diphenylanthracene and PPM. The first oxidation potential of 9,10-diphenylanthracene arises at ~1.0 V, whereas for PPM the corresponding feature appears at ~1.7 V (see Figure S5 in the Supporting Information). Furthermore, the UV-Vis spectrum of 9,10-diphenylanthracene differs considerably from that of PPM (see Figure S11 in the Supporting Information).

Finally, if a 9,10-diphenylanthracene impurity was indeed responsible for the observed fluorescence then the spectral red-shift with increasing molar mass reported in Figure 3 would *not* be observed since the extent of electronic delocalization would be virtually independent of the length of the attached poly(phenylene methylene) chain segments.

Overall, the considerations presented above do not support the proposal that the unexpected fluorescent properties of PPM and its derivatives originate from the presence of a 9,10-diphenylanthracene (or a related) impurity. Further evidence for this is presented in the following section.

Homoconjugation

Previously it has been proposed that π-orbitals of aromatic groups separated by a methylene group (or other groups with comparable geometry) can overlap – a phenomenon which is rarely considered[68-72] – and hence establish a conjugation over two C-C single bonds. This phenomenon is termed *homoconjugation*.[17,18] While homoconjugation has been reported for low-molar-mass organic molecules,[19,73,74] we are not aware of any such reports for polymers, which is not surprising given that the majority of known polymers rarely fulfil the structural requirements for homoconjugation. Homoconjugation in PPM would involve the π-orbitals from the substituted carbon atoms (C_{sub}) of a phenylene ring as the π-orbitals capable of overlapping with those of C_{sub} atoms on the adjacent phenylene rings, as illustrated schematically in **Figure 6**(a).

As a confirmation that homoconjugation can occur in PPM, structural analysis of diphenylmethane, which can be regarded as analogous to a PPM chain segment, revealed that the C_{sub}-C_{sub} distance of ~2.6 Å is smaller than the sum of the corresponding van der Waals radii (~3.4 Å).[72,75] Furthermore, a slightly tilted cofacial conformation of diphenylmethane in terms of the two phenyl rings (point group C_2) was found to be energetically the most favored conformation compared with orthogonal (point group C_s) or even perfect cofacial conformations (point group C_{2v}).[75–77] Density functional theory (DFT) calculations performed for a para-substituted PPM (quasi) dimer (see Figure 6(b)) confirm that the

lowest energy conformation has a dihedral angle of ~56° with respect to the molecular plane (defined by C_{sub}-CH_2-C_{sub}). The corresponding HOMO and LUMO for this conformation are shown in Figure 6(c) and, most importantly, indicate for the LUMO a clear delocalization of electron density across the adjacent phenylene rings.[78] Overall, these findings demonstrate that the principal structural requirements for homoconjugation in PPM are satisfied.

It is apparent, therefore, that homoconjugation in PPM and its derivatives would require the polymer chains to adopt a precisely-defined conformation in terms of the spatial orientation between adjacent repeat units (see Figure 6), which, in fact, is indirectly corroborated by the high degree of vibronic resolution in the optical spectra. Although DFT calculations indicated this conformation to be the most energetically favorable for PPM, its formation would be hindered by kinetic factors determined by, for instance, deposition conditions and reduction in chain mobility due to macromolecular entanglements. Conversely, if the influence of kinetic factors is ameliorated by, e.g., post-deposition thermal annealing above T_g (resulting in increased mobility of chain segments), the formation of homoconjugated chain segments in PPM would be promoted.

To confirm this experimentally, absorption measurements were taken for a PPM sample during annealing, with the results presented in **Figure 7**. For the initial sample, as-synthesized PPM powder was pressed into a disk-shaped plaque (cf. inset in Figure 7) at room temperature – that is, *below* T_g of PPM. The polymer chains in this sample are expected to possess *maximally disordered conformations* due to the rapidly-occurring precipitation conditions used to obtain the polymer powder after synthesis. The PPM plaque was mounted on a fused silica substrate and absorption measurements were performed in an integrating sphere (thus eliminating the effects of scattering) at excitation wavelengths λ_{ex} = 280 nm (*localized* absorption of phenylene) and 366 nm (*delocalized* S_0-S_1 0-2 vibronic peak of the *blue*-phase of PPM). In all cases, absorption was calculated from the attenuation of the excitation peak relative to a pristine fused silica substrate acting as a 'zero-absorption' reference, i.e. analogous to the procedure used for the PLQE measurements reported above.[46]

The PPM plaque was sequentially annealed for 5 min in an inert atmosphere glovebox at selected temperatures, and absorption measurements were performed after each annealing step. It is shown in Figure 7 that absorption at 366 nm undergoes a step-increase of ~25% when the annealing temperature exceeds the T_g of PPM, confirming the proposal that the population of homoconjugated chain segments in PPM increases upon 'equilibration' of the polymer chain ensemble via thermal annealing. Conversely, absorption at 280 nm remains virtually constant, exhibiting only a ~3% decrease above T_g, plausibly due to a minor transfer of oscillator strength. The intense yellow color of the PPM plaque which emerges after annealing above T_g (cf. inset in Figure 7) is fully consistent with increased absorption in the 350 nm – 450 nm spectral region. Gratifyingly, the same experiment performed for PTMPM yielded matching results, albeit with the increase in delocalized absorption occurring at the higher T_g of 147 °C (cf. Table 1; data not shown).

We note that the different trends seen for absorption at 280 nm and 366 nm as a function of temperature exclude changes in light-scattering as the origin of the observations in Figure 7. Furthermore, the observed increase in absorption at 366 nm upon annealing rules out the possibility that the optical properties of PPM are due to a *fixed* population of 9,10-diphenyanthracene (or other) impurities.

Given the analysis presented above, we conclude that homoconjugation in PPM and its methyl-substituted derivatives is in agreement with all experimental results, in contrast to the other potential origins discussed.

CONCLUSION

The polymerization of benzyl chloride was optimized to yield materials with molar masses in the range of 10'000 g mol^{-1}, and 2-methylbenzyl chloride and 2,4,6-trimethylbenzyl chloride were polymerized accordingly. The resulting polymers (PPM, PMPM and PTMPM, respectively) exhibit pronounced blue fluorescence in solutions as well as films despite the absence of π-conjugation between adjacent

repeat units. Optical spectroscopy was used extensively to explore the characteristics and, specifically, the origin of the unexpected fluorescent properties of PPM and its derivatives.

It was shown that solid-state PPM exhibits a remarkably long photoluminescence (PL) lifetime (>8 ns) and relatively high photoluminescence quantum efficiency (41%), and possesses two discrete optically-active species, termed *blue*- and *green*-phase herein. Temperature-dependent optical spectroscopy, as well as thermal and X-ray diffraction analyses, indicate that the optical properties of PPM are not due to π-stacking or aggregation/crystallization. Electronic delocalization *along* the polymer chain is confirmed by the observation of PL spectral red-shift with increasing molar mass of PPM. Accordingly – in contrast to the earlier reports – it is concluded that the presence of 9,10-diphenylanthracene (or other) impurities is *not* the origin of the fluorescent properties in PPM.

On the contrary, here is sufficient evidence that the origin of the optical properties of PPM and its derivatives (absorption in the 350 nm – 450 nm and photoluminescence in the 400 nm – 600 nm spectral regions) is *homoconjugation*, i.e. π-orbital overlap across adjacent repeat units enabled by a particular chain conformation. DFT calculations confirm that the principal structural requires for homoconjugation in PPM are satisfied.

Our findings, therefore, demonstrate, to the best of our knowledge, the first instance of fluorescence enabled by *homoconjugation* in macromolecular compounds and thereby open new pathways for the design of next-generation light-emitting polymers with hitherto unknown optical properties.

EXPERIMENTAL

Materials

Chemicals were purchased from the following companies: Tin(IV) chloride, benzyl chloride (99%), chloroform, tetrahydrofuran (THF) and toluene from Sigma-Aldrich (Buchs, Switzerland); benzyl chloride (99.5%), 2-methylbenzyl chloride (99%) and 2,4,6-trimethylbenzyl chloride (98%) from Acros

Organics (Reinach, Switzerland). With the exception of benzyl chloride (see below), all chemicals were used as received.

Synthesis of Poly(phenylene methylene) (PPM) with higher molar mass

First, benzyl chloride was exposed to vacuum (~10^{-2} mbar) for 12 h to remove the propylene oxide stabilizer (0.25% w/v). The removal of the stabilizer was verified by ^{1}H-NMR spectroscopy (disappearance of signals at 2.96 ppm, 2.73 ppm, 2.41 ppm and 1.31 ppm). The destabilized benzyl chloride (95 mL, 825 mmol) was transferred under a nitrogen atmosphere into a 250 mL three-neck round-bottom flask equipped with a mechanical glass stirrer. $SnCl_4$ (1.2 mL, 10.3 mmol) was then added to the benzyl chloride at room temperature under stirring. Subsequently, the solution was heated to 80 °C. Polymerization was carried out under a constant nitrogen flow rate of 17 mL min^{-1} to allow the produced HCl to escape. Due to increased viscosity after 2 h, the temperature was increased to 120 °C for another 2 h and subsequently to 140 °C for 16 h. The evolution of color during the reaction was as follows: clear orange, deep red (opaque), clear amber and eventually clear green-yellow. The resulting reaction mixture was allowed to cool down to room temperature and dissolved in 200 mL of THF, precipitated into 1.5 L of methanol, filtered (cellulose filter) and dried under vacuum (10^{-2} mbar, 18 h) to give 70.1 g (94%) of PPM. ^{1}H-NMR (300 MHz, $CDCl_3$, δ): 3.79 (br, 2H), 7.05 (br, 4H); elemental analysis: $[C_7H_6]_n$ (molar mass: 90.12 g mol^{-1}; calculated values in brackets, in % m/m): C 93.32% (93.29%), H 6.63% (6.71%). ICP-OES: Sn content below the detection limit of 0.025 ppm; GPC ($CHCl_3$): M_n = 10'900 g mol^{-1}, M_w = 35'900 g mol^{-1}, M_w/M_n = 3.3; DSC (T_g): 66 °C. *N.B.* Benzyl chloride from Acros Organics (99.5% purity) was used for the synthesis of the products investigated above; however, selected experiments using benzyl chloride from Sigma-Aldrich (99% purity) were found to yield materials with virtually identical characteristics (^{1}H NMR spectra, T_g and, in qualitative terms, fluorescence spectra).

Synthesis of PPM with lower molar mass

Under nitrogen atmosphere, 50 mL (434 mmol) of destabilized benzyl chloride (cf. synthesis of PPM of higher molar mass) was transferred into a 250 mL three-neck round-bottom flask equipped with a mechanical glass stirrer. After heating benzyl chloride to 80 °C, 0.1 mL (0.86 mmol) of $SnCl_4$ was added. Subsequently, small portions of ca. 3 g were taken out of the reaction vessel every 10 min. These portions were then dissolved immediately in chloroform (5 mL), precipitated into 100 mL of methanol, filtered through a cellulose filter and finally dried under vacuum (~10^{-2} mbar, 12 h). Due to increased viscosity after 100 min, the temperature of the remaining reaction mixture was increased to 120 °C for 2 h and then to 140 °C for another 14 h. The entire process was carried out under a constant nitrogen flow rate of 17 mL min^{-1} to allow the produced HCl to escape. The evolution of color during the reaction was as follows: clear orange, deep red (opaque), clear amber and eventually clear green-yellow. The resulting reaction mixture was allowed to cool down to room temperature and dissolved in 40 mL of chloroform, precipitated into 350 mL of methanol, filtered through a cellulose filter and dried under vacuum (10^{-2} mbar, 18 h). The degree of polymerization (DP) was evaluated by ^{1}H-NMR spectroscopy[79,80] (see *Results*).

Synthesis of Poly(2-methylphenylene methylene) (PMPM)

Under nitrogen atmosphere, 2-methylbenzyl chloride (44.5 mL, 336 mmol) was transferred into a 100 mL three-neck round-bottom flask equipped with a mechanical glass stirrer. $SnCl_4$ (0.3 mL, 2.6 mmol) was then added to the 2-methylbenzyl chloride at room temperature under stirring. Subsequently, the reaction mixture was heated to 80 °C. Polymerization was carried out under a constant nitrogen flow rate of 17 mL min^{-1} to allow the produced HCl to escape. Due to increased viscosity after 60 min, the temperature was increased to 120 °C for another 60 min and then to 200 °C for 150 min. The evolution of color during the reaction was as follows: clear orange, deep red (opaque), clear pink and eventually clear pale yellow. The resulting reaction mixture was allowed to cool down to room temperature and dissolved in 60 mL of THF, precipitated into 1000 mL of methanol, filtered through a cellulose filter and dried under vacuum (10^{-2} mbar, 18 h) to give 34.5 g (97%) of PMPM. ^{1}H-NMR (300 MHz, $CDCl_3$, δ): 2.09 (br, 3H), 3.77 (br, 2H), 6.81-7.08 (br, 3H); elemental analysis: $[C_8H_8]_n$ (molar mass: 104.2 g mol^{-1};

calculated values in brackets, in % m/m): C 92.23% (92.26%), H 7.67% (7.74%); GPC ($CHCl_3$): M_n = 10'500 g mol^{-1}, M_w = 52'900 g mol^{-1}, M_w/M_n = 5.0; DSC (T_g): 93 °C.

Synthesis of Poly(2,4,6-trimethylphenylene methylene) (PTMPM)

Under a nitrogen atmosphere, in a 50 mL three-neck round-bottom flask equipped with a mechanical glass stirrer 2,4,6-trimethylbenzyl chloride (8140 mg, 48.26 mmol) was heated to 50 °C in order to melt it. $SnCl_4$ (25 µL, 0.21 mmol) was then added under stirring and the reaction mixture was kept at 50 °C for 15 min. Subsequently, the reaction mixture was heated to 200 °C for 20 min due to increased viscosity. Polymerization was carried out under a constant nitrogen flow rate of 17 mL min^{-1} to allow the produced HCl to escape. The evolution of color during the reaction was as follows: clear orange, deep red (opaque), clear amber and eventually clear yellow. After 30 min at 200 °C, the resulting reaction mixture was allowed to cool down to room temperature and dissolved in 18 mL of THF, precipitated into 330 mL of methanol, filtered through a cellulose filter and dried under vacuum (10^{-2} mbar, 24 h) to give 5.67 g (88.8%) of PTMPM. ^{1}H-NMR (300 MHz, $CDCl_3$, δ): 1.81–2.34 (m, 9H), 3.88 (br, 2H), 6.66-7.79 (m, 1H); elemental analysis: $[C_{10}H_{12}]_n$ (molar mass: 132.2 g mol^{-1}; calculated values in brackets, in % m/m): C 89.78% (90.85%), H 9.21% (9.15%); GPC ($CHCl_3$): M_n = 5'000 g mol^{-1}, M_w = 27'300 g mol^{-1}, M_w/M_n = 6.1; DSC (T_g): 147 °C.

Film fabrication

Films of PPM and its derivatives were spin-coated onto fused silica substrates (Spectrosil B®, UQG Optics Ltd). Thin films (thickness ~330 nm) were deposited from 834 mmol L^{-1} (~4.8% m/m) solutions in chloroform using ~10000 rpm spin rates. Thick films (thickness ~17 µm) were deposited from 50% m/m solutions in toluene using ~2000 rpm spin rates, with both solution and substrates pre-heated to 90 °C immediately prior to spin-coating. Thickness of films was determined using a KLA-Tencor P11 profilometer. *N.B.* All molar concentrations herein refer to the respective constitutional repeat units of the polymers.

Characterization

^{1}H-NMR spectra were recorded on a Bruker AV300 MHz instrument using $CDCl_3$ as the solvent. Elemental analysis was performed at the Microanalytic Laboratory of the Laboratory of Organic Chemistry (LOC), ETH Zürich. Inductively coupled plasma optical emission spectrometry (ICP-OES) with a typical detection limit of 0.025 ppm was performed by Sika Technologies AG (Switzerland) using nitric acid and hydrochloric acid for the digestion matrix. Analytical gel permeation chromatography (GPC) measurements were performed using a Viscotek GPC system equipped with a pump and a degasser (GPCmax VE2001; 1.0 mL min^{-1} flow rate), a detector module (Viscotek 302 TDA) and three columns (2× PLGel Mix-C and 1× ViscoGEL GMHHRN 18055; dimensions 7.5 mm × 300 mm for each column) using chloroform as an eluent.

Thermogravimetric analysis (TGA) was performed using a Mettler Toledo TGA/SDTA851^e instrument, with the samples heated from 25 °C to 1100 °C at a rate of 10 °C min^{-1} under both ambient and nitrogen atmospheres. Differential scanning calorimetry (DSC) was carried out using a Mettler Toledo DSC822^e instrument routinely calibrated against indium standards. Standard 10 °C min^{-1} heating/cooling rates were used, with all measurements performed under a nitrogen blanket.

Cyclic voltammetry (CV) was performed under an inert N_2 atmosphere in a glove box in dry solvents with a Gamry Instruments Reference 600 Potentiostat using a three electrode setup. Glassy carbon was used as the working electrode and Pt wire (99.99%) as the supporting electrode; the reference electrode was a Ag wire immersed in a solution of 0.01 M $AgNO_3$ and 0.1 M $(NBu_4)PF_6$ in CH_3CN separated from the solution by a Vycor® tip. Voltammograms were finally referenced to ferrocene/ferrocenium ($E_{1/2}$ = 0.1 V with the same setup). Supporting electrolyte used was $(NBu_4)PF_6$. IR compensation was applied. Electrochemical measurements were performed in dichloromethane (~30 mmol L^{-1}) from –2.5 V to +2.5 V at a scan rate of 20 mV s^{-1}. The energy values for the HOMO and LUMO levels were calculated using the ferrocene value of –4.8 eV[37,81] according to the following equations: HOMO = –($E_{\mathrm{ox,onset}}$ + 4.8) eV and LUMO = –($E_{\mathrm{red,onset}}$ + 4.8) eV.[82,83]

Wide-angle X-ray diffraction was performed on an Oxford Instruments XCalibur PX diffractometer using Mo-Kα radiation (wavelength = 0.71 Å). Polymer samples were sealed inside glass capillary tubes (Hilgenberg GmbH, Germany), the temperature of which was controlled using the instrument's Cryojet accessory.

Photoluminescence (PL) and photoluminescence excitation (PLE) measurements were performed using a 90°-optical geometry Jasco FP-8500 spectrofluorometer. PL and PLE spectroscopy of film samples was carried out at room temperature, with the films positioned to provide a 30° angle between the excitation beam and the normal to film plane. For temperature-dependent measurements on solutions, the instrument was equipped with a thermostatted cuvette holder (ETC-815). Solutions were placed in 10×10 mm quartz cuvettes (Hellma Analytics, Germany). Photoluminescence quantum efficiency (PLQE) measurements as well as temperature-dependent absorption measurements on the cold-pressed, as-synthesized PPM powder samples were performed using a HORIBA Scientific FluoroMax-4 spectrofluorometer equipped with the Quanta-φ integrating sphere attachment. Self-absorption correction in the PLQE analysis was carried out using the method described in Refs. [46,84]

Room-temperature UV-Vis absorption spectra were recorded using a Jasco V-660 spectrophotometer. Solutions were placed in 10×10 mm cuvettes (as above). For measurements on spin-coated films, the instrument was equipped with a diffuse reflectivity attachment (ILN-725), allowing the resulting spectra to be corrected for specular reflection and scattering losses. Temperature-dependent UV-Vis absorption spectroscopy measurements on solutions were performed using a Shimadzu UV-1601 spectrophotometer equipped with a thermostatted cuvette holder. Solutions were placed inside 10×10 mm cuvettes (as above) and transmission spectra were recorded at each chosen temperature for both PPM solutions and the neat solvent.

PL transients were measured for PPM films (thickness ~330 nm) using a streak camera system (Hamamatsu Photonics C4334) coupled to a spectrometer (Hamamatsu Photonics C5094) with

excitation at 379 nm (60 ps pulses, 1 MHz repetition rate). Fluorescence from the sample was directed to the streak camera via a monochromator, and photon-counting events were recorded as a function of both time and emission wavelength.

Density functional theory (DFT) calculations were performed with the GAUSSIAN09 software using a B3LYP functional and the 6-31G basis set.

ACKNOWLEDGEMENTS

We express our deep gratitude to Prof. em. Paul Smith, Prof. Dieter Schlüter and Dr. Alessandro Lauria (ETH Zürich) as well as Prof. Donal Bradley (University of Oxford) for helpful discussions and valuable advice concerning the present paper. We also thank Yiren Xia (Imperial College London) for performing the streak-camera measurements, as well as Jonas Kissling (Sika Technologies AG, Switzerland) for ICP-OES analysis. The financial support of the Swiss National Science Foundation (No. 200021_159719 / 1) is acknowledged.

REFERENCES

1. N. Harrison, D. Baigent, I. Samuel, R. Friend, A. Grimsdale, S. Moratti, A. Holmes, *Phys. Rev. B* **1996**, *53*, 15815.
2. G. E. Wnek, J. C. W. Chien, F. E. Karasz, C. P. Lillya, *Polym. Commun.* **1979**, *20*, 1441.
3. S. Heun, R. F. Mahrt, A. Greiner, U. Lemmer, H. Bässler, D. A. Halliday, D. D. C. Bradley, P. L. Burn, A. B. Holmes, *J. Phys. Condens. Matter* **1993**, *5*, 247.
4. D. Neher, *Macromol. Rapid Commun.* **2001**, *22*, 1365.
5. A. Perevedentsev, Y. Sonnefraud, C. R. Belton, S. Sharma, A. E. G. Cass, S. A. Maier, J.-S. Kim, P. N. Stavrinou, D. D. C. Bradley, *Nat. Commun.* **2015**, *6*, 5977.
6. A. Perevedentsev, P. N. Stavrinou, P. Smith, D. D. C. Bradley, *J. Polym. Sci. Part B Polym. Phys.* **2015**, *53*, 1492.
7. I. F. Perepichka, D. F. Perepichka, H. Meng, F. Wudl, *Adv. Mater.* **2005**, *17*, 2281.
8. X. M. Jiang, R. Österbacka, O. Korovyanko, C. P. An, B. Horovitz, R. A. J. Janssen, Z. V. Vardeny,

Adv. Funct. Mater. **2002**, *12*, 587.

9. C. W. Frank, L. A. Harrah, *J. Chem. Phys.* **1974**, *61*, 1526.
10. G. G. Nossarev, J. Johnson, S. E. Bradforth, T. E. Hogen-Esch, *J. Phys. Chem. C* **2013**, *117*, 10244.
11. I. Natori, S. Natori, H. Sekikawa, T. Takahashi, H. Sato, *J. Appl. Polym. Sci.* **2010**, *118*, 69.
12. P. V. Kamat, *Anal. Chem.* **1987**, *59*, 1636.
13. B. Valeur, M. N. Berberan-Santos, *Molecular Fluorescence*; Wiley-VCH: Weinheim, Germany, 2012.
14. D. Wang, T. Imae, M. Miki, *J. Colloid Interface Sci.* **2007**, *306*, 222.
15. W. I. Lee, Y. Bae, A. J. Bard, *J. Am. Chem. Soc.* **2004**, *126*, 8358.
16. M. Simonetta, S. Winstein, *J. Am. Chem. Soc.* **1954**, *76*, 18.
17. L. T. Scott, *Pure Appl. Chem.* **1986**, *58*, 105.
18. P. Muller, *Pure Appl. Chem.* **1994**, *66*, 1077.
19. L. N. Ferguson, J. C. Nnadi, *J. Chem. Educ.* **1965**, *42*, 529.
20. B. Ellis, P. G. White, R. N. Young, *Eur. Polym. J.* **1969**, *5*, 307.
21. D. Gunes, Y. Yagci, N. Bicak, *Macromolecules* **2010**, *43*, 7993.
22. D. B. V. Parker, *Eur. Polym. J.* **1969**, *5*, 93.
23. Cannizzaro S., *Justus Liebigs Ann. Chem.* **1853**, *88*, 129.
24. L. Valentine, R. W. Winter, *J. Chem. Soc.* **1956**, *0*, 4768.
25. D. B. V. Parker, W. G. Davies, K. D. South, *J. Chem. Soc. B Phys. Org.* **1967**, *0*, 471.
26. J. Kuo, R. W. Lenz, *J. Polym. Sci. Polym. Chem. Ed.* **1976**, *14*, 2749.
27. G. Montaudo, P. Finocchiaro, S. Caccamese, F. Bottino, *J. Polym. Sci. Part A-1 Polym. Chem.* **1970**, *8*, 2475.
28. R. A. Jacobson, *J. Am. Chem. Soc.* **1932**, *54*, 1513.
29. P. J. Blincow, G. Pritchard, *Polymer* **1987**, *28*, 1824
30. M. Ul Hasan, C. P. Tsonis, *J. Polym. Sci. Polym. Chem. Ed.* **1984**, *22*, 1349.

31. H. C. Haas, D. I. Livingston, M. Saunders, *J. Polym. Sci.* **1955**, *15*, 503.

32. I. Olliges-Stadler, M. D. Rossell, M. Niederberger, *Small* **2010**, *6*, 960.

33. F. Böttger-Hiller, R. Lungwitz, A. Seifert, M. Hietschold, M. Schlesinger, M. Mehring, S. Spange, *Angew. Chemie Int. Ed.* **2009**, *48*, 8878.

34. F. B. F. Silva, E. C. Paris, G. M. da Costa, C. Ribeiro, *RSC Adv.* **2014**, *4*, 53265.

35. T. M'Hiri, C. Catusse, R. Catusse, J. L. Janier Dubry, *React. Kinet. Catal. Lett.* **1983**, *22*, 425.

36. M. Hino, K. Arata, *Chem. Lett.* **1979**, *8*, 1141.

37. Y. Liu, M. S. Liu, A. K.-Y. Jen, *Acta Polym.* **1999**, *50*, 105.

38. W. C. Neikam, G. R. Dimeler, M. M. Desmond, *J. Electrochem. Soc.* **1964**, *111*, 1190.

39. Z. Blum, L. Cedheim, L. Eberson, V. D. Parker, A. Christensen, G. Schroll, *Acta Chem. Scand.* **1977**, *31b*, 662.

40. D. D. Tunnicliff, R. R. Brattain, L. R. Zumwalt, *Anal. Chem.* **1949**, *21*, 890.

41. A. Köhler, S. T. Hoffmann, H. Bässler, *J. Am. Chem. Soc.* **2012**, *134*, 11594.

42. H. Yamagata, N. J. Hestand, F. C. Spano, A. Köhler, C. Scharsich, S. T. Hoffmann, H. Bässler, *J. Chem. Phys.* **2013**, *139*, 114903.

43. D. Hertel, U. Scherf, H. Bässler, *Adv. Mater.* **1998**, *10*, 1119.

44. U. Scherf, E. J. W. List, *Adv. Mater.* **2002**, *14*, 477.

45. F. Panzer, M. Sommer, H. Bässler, M. Thelakkat, A. Köhler, *Macromolecules* **2015**, *48*, 1543.

46. A. Perevedentsev, P. N. Stavrinou, D. D. C. Bradley, P. Smith, *J. Polym. Sci. Part B Polym. Phys.* **2015**, *53*, 1481.

47. J. Cornil, D. Beljonne, Z. Shuia, T. W. Hagler, I. Campbell, D. D. C. Bradley, J. L. Brédas, C. W. Spangler, K. Müllen, *Chem. Phys. Lett.* **1995**, *247*, 425.

48. S. Tirapattur, M. Belletête, N. Drolet, M. Leclerc, G. Durocher, *Macromolecules* **2002**, *35*, 8889.

49. A. K. Bansal, A. Ruseckas, P. E. Shaw, I. D. W. Samuel, *J. Phys. Chem. C* **2010**, *114*, 17864.

50. A. Cadby, R. Dean, A. M. Fox, R. A. L. Jones, D. G. Lidzey, *Nano Lett.* **2005**, *5*, 2232.

51. K. Kanemoto, M. Shishido, T. Sudo, I. Akai, H. Hashimoto, T. Karasawa, *Chem. Phys. Lett.* **2005**, *402*, 549.

52. W. Chen, X. Sun, X. Wang, Q. Huang, X. Li, Q. Zhang, J. Jiang, G. Zhang, *Polym. Chem.* **2015**, *6*, 1698.

53. L. M. Herz, R. T. Phillips, *Phys. Rev. B* **2000**, *61*, 13691.

54. M. Kasha, H. R. Rawls, M. Ashraf El-Bayoumi, *Pure Appl. Chem.* **1965**, *11*, 371.

55. S. S. Yanari, F. A. Bovey, R. Lumry, *Nature* **1963**, *200*, 242.

56. M. Sims, D. D. C. Bradley, M. Ariu, M. Koeberg, A. Asimakis, M. Grell, D. G. Lidzey, *Adv. Funct. Mater.* **2004**, *14*, 765.

57. H. Liu, L. Yao, B. Li, X. Chen, Y. Gao, S. Zhang, W. Li, P. Lu, B. Yang, Y. Ma, *Chem. Commun.* **2016**, *52*, 7356.

58. J. Mei, Y. Hong, J. W. Y. Lam, A. Qin, Y. Tang, B. Z. Tang, *Adv. Mater.* **2014**, *26*, 5429.

59. T. Nakano, *Polym. J.* **2010**, *42*, 103.

60. D. L. Dexter, J. H. Schulman, *J. Chem. Phys.* **1954**, *22*, 1063.

61. T. Forster, *Ann. Phys.* **1948**, *2*, 55.

62. R. Hu, N. L. C. Leung, B. Z. Tang, *Chem. Soc. Rev.* **2014**, *43*, 4494.

63. Y. Hong, J. W. Y. Lam, B. Z. Tang, *Chem. Soc. Rev.* **2011**, *40*, 5361.

64. F. Würthner, T. E. Kaiser, C. R. Saha-Möller, *Angew. Chemie Int. Ed.* **2011**, *50*, 3376.

65. Y. Ashikari, T. Nokami, J. Yoshida, *J. Am. Chem. Soc.* **2011**, *133*, 11840.

66. R. P. A. Sneeden, H. H. Zeiss, *J. Organometal. Chem.* **1969**, *16*, 449.

67. I. B. Berlman, *Handbook of Fluorescence Spectra of Aromatic Molecules*; Academic Press INC.: New York City, NJ, USA, 1971.

68. J. O. Barcina, M. D. R. C. Heras, M. Mba, R. G. Aspe, N. H. García, *J. Org. Chem.* **2009**, *74*, 7148.

69. J. O. Barcina, N. G. Herrero, F. Cucinotta, L. De Cola, P. C. Carballada, R. M. Williams, A. G. Martínez, *Chem. - A Eur. J.* **2010**, *16*, 6033.

70. A. G. Martínez, J. O. Barcina, A. de F. Cerezo, R. G. Rivas, *J. Am. Chem. Soc.* **1998**, *120*, 673.

71. A. G. Martínez, J. O. Barcina, A. de F. Cerezo, A.-D. Schlüter, J. Frahn, *Adv. Mater.* **1999**, *11*, 27.

72. N. C. Martínez, M. del R. C. Heras, M. M. Blázquez, J. O. Barcina, A. G. Martínez, M. del R. T. Salvador, *Org. Lett.* **2007**, *9*, 2943.

73. H.-D. Martin, B. Mayer, *Angew. Chemie Int. Ed. English* **1983**, *22*, 283.

74. L. A. Paquette, *Angew. Chemie Int. Ed. English* **1978**, *17*, 106.

75. J. C. Barnes, J. D. Paton, J. R. Damewood, K. Mislow, *J. Org. Chem.* **1981**, *46*, 4975.

76. T. Strassner, *Can. J. Chem* **1997**, *75*, 1011.

77. J. A. Stearns, N. R. Pillsbury, K. O. Douglass, C. W. Müller, T. S. Zwier, D. F. Plusquellic, *J. Chem. Phys.* **2008**, *129*, 224305.

78. T. Kobayashi, S. Kobayashi, *European J. Org. Chem.* **2002**, *2002*, 2066.

79. H. W. G. van Herwijnen, U. H. Brinker, *Tetrahedron* **2002**, *58*, 4963.

80. H. W. G. van Herwijnen, U. H. Brinker, *J. Org. Chem.* **2001**, *66*, 2874.

81. P. Deng, L. Liu, S. Ren, H. Li, Q. Zhang, *Chem. Commun.* **2012**, *48*, 6960.

82. J. L. Brédas, R. Silbey, D. S. Boudreaux, R. R. Chance, *J. Am. Chem. Soc.* **1983**, *105*, 6555.

83. D. M. de Leeuw, M. M. J. Simenon, A. R. Brown, R. E. F. Einerhand, *Synth. Met.* **1997**, *87*, 53.

84. T.-S. Ahn, R. O. Al-Kaysi, A. M. Müller, K. M. Wentz, C. J. Bardeen, *Rev. Sci. Instrum.* **2007**, *78*, 86105.

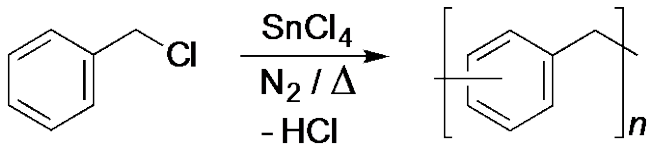

Scheme 1: Synthesis of poly(phenylene methylene) (PPM).

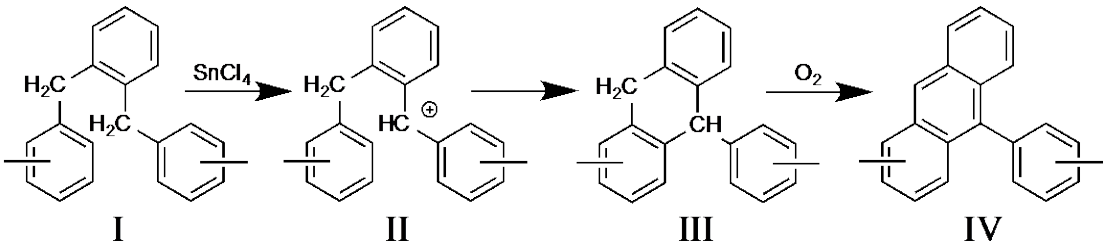

Scheme 2: Formation of diphenylanthracene as proposed in the literature (see text). Scheme adapted from Ref. [20]**.**

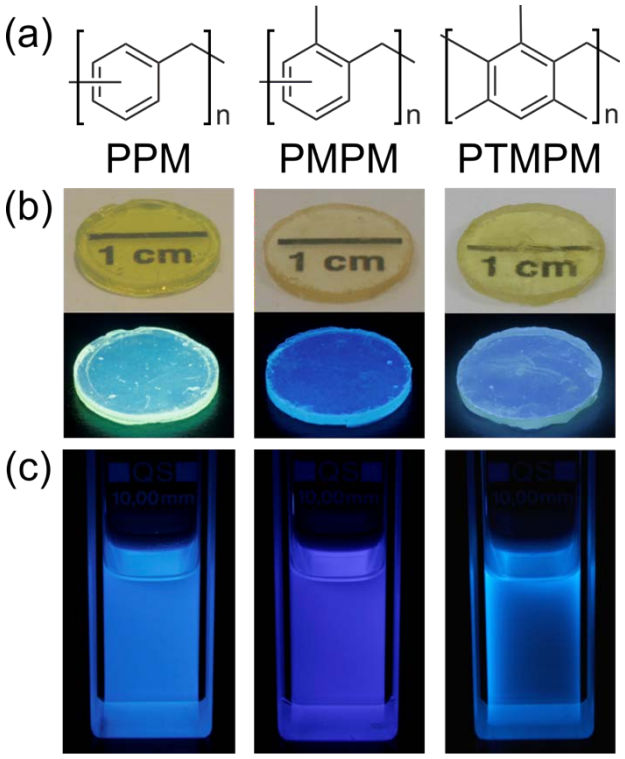

Figure 1. Left column: PPM, center column: PMPM, right column: PTMPM. (a) Chemical structures, (b) photographs, taken under white-light (above) and UV-light (~365 nm) illumination (below), of polymer plaques (~1.2 mm thickness; pressed at $\boldsymbol{T} > \boldsymbol{T}_{\mathbf{g}}$), (c) photographs taken under UV-light illumination of polymer solutions in chloroform (PPM: 83 mmol L^{-1}; PMPM: 71 mmol L^{-1}; PTMPM: 28 mmol L^{-1}).

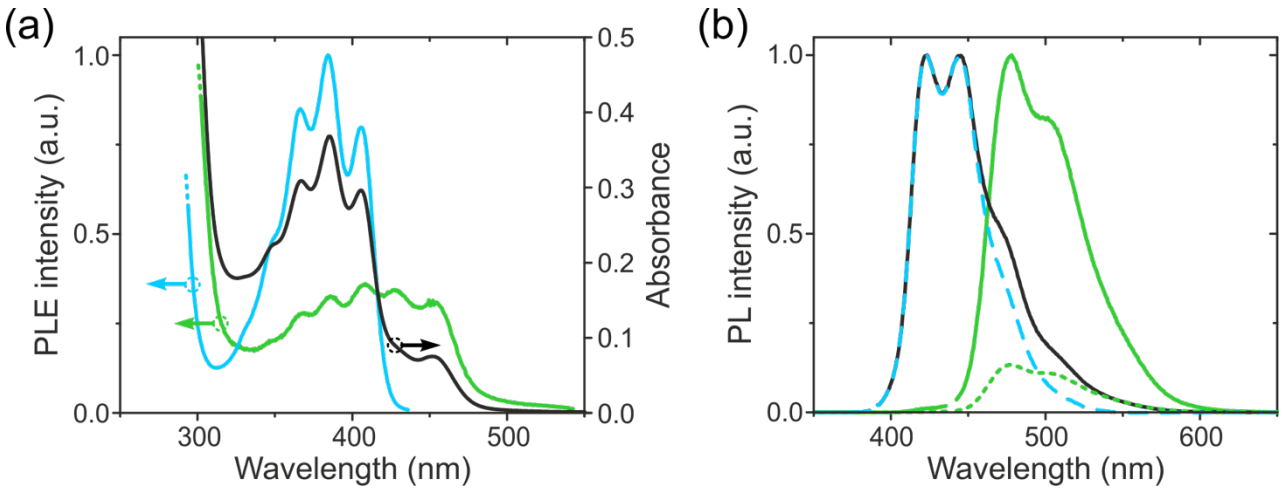

Figure 2. Optical spectra of PPM in a semi-dilute (83 mmol L^{-1}) solution in chloroform. (a) Absorption (black line, right ordinate) and PLE spectra (left ordinate) for emission detected at 445 nm (blue line) and 550 nm (green line). (b) Peak-normalized PL spectra excited at 388 nm (solid black line; '*total PL*') and 438 nm (solid green line; '*green-phase PL*'). The 'total PL' spectrum comprises a superposition of the *blue*-phase ('*blue-phase PL*'; dashed blue line) and the *green*-phase PL spectra (dotted green line).

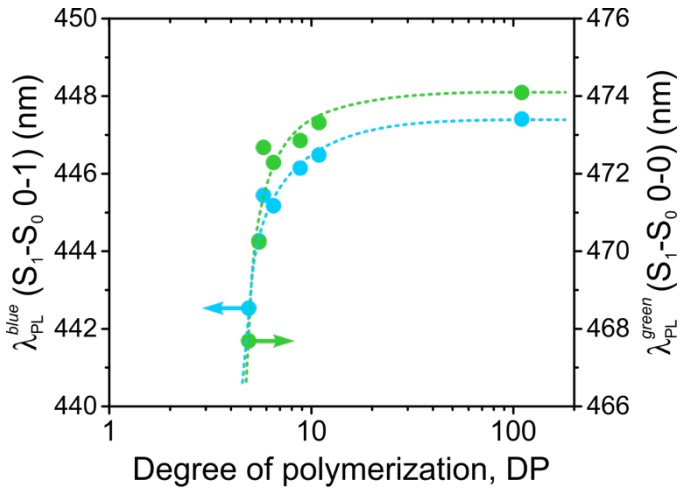

Figure 3. Variation of S_1-S_0 PL wavelengths, λ_{PL}, corresponding to the *blue*-phase 0-1 (blue circles; left ordinate) and *green*-phase 0-0 (green circles; right ordinate) vibronic peaks with the average degree of polymerization of PPM. Data recorded for room-temperature solutions in chloroform. Dotted lines represent a guide for the eye only.

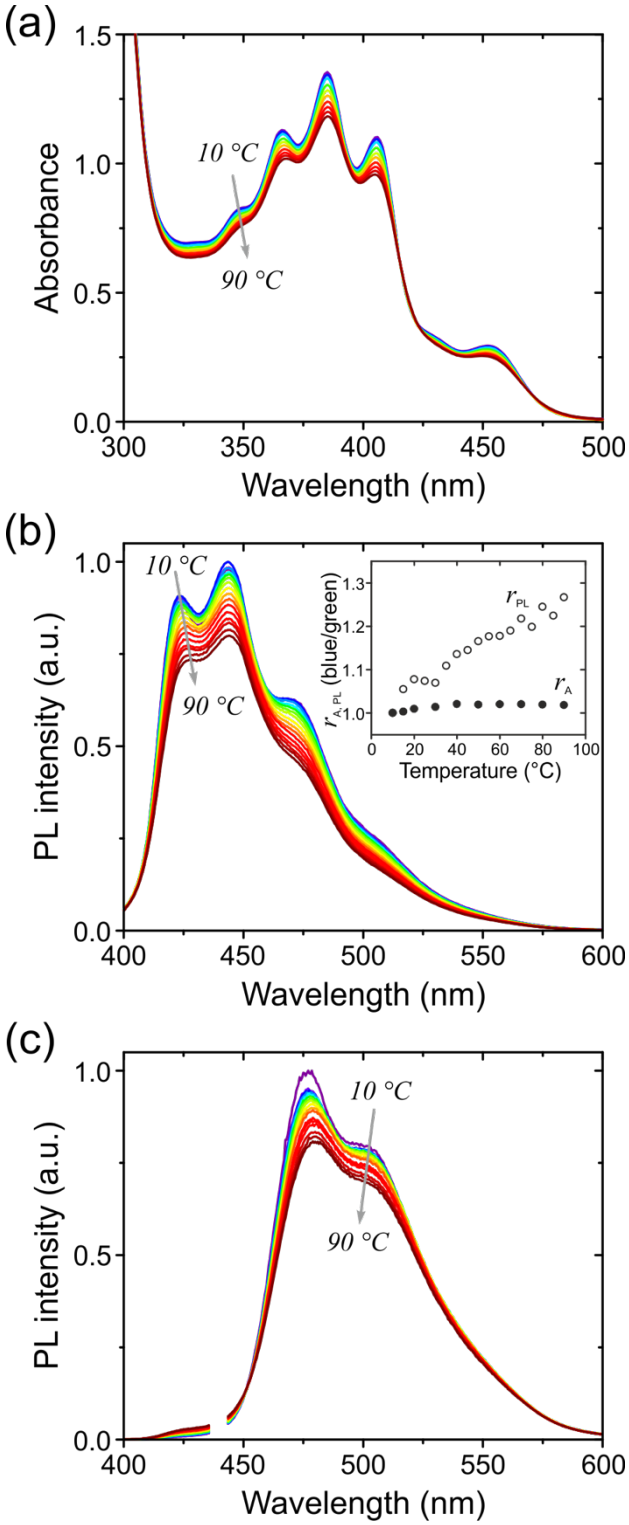

Figure 4. Temperature-dependent optical spectra of PPM solutions in toluene (289 mmol L^{-1}) upon heating from 10 °C to 90 °C in 5 °C or 10 °C increments; arrows indicate the direction of spectral changes. (a) Absorption spectra and (b,c) PL spectra excited at (b) 388 nm and (c) 438 nm. The inset in (b) shows the temperature-dependent evolution of the *blue*- to *green*-phase absorbance ratio, r_{A}, (●) and integrated PL intensity ratio for the 'total' PL spectrum, r_{PL}, (○), with both datasets normalized by the respective values at 10 °C (see text for details).

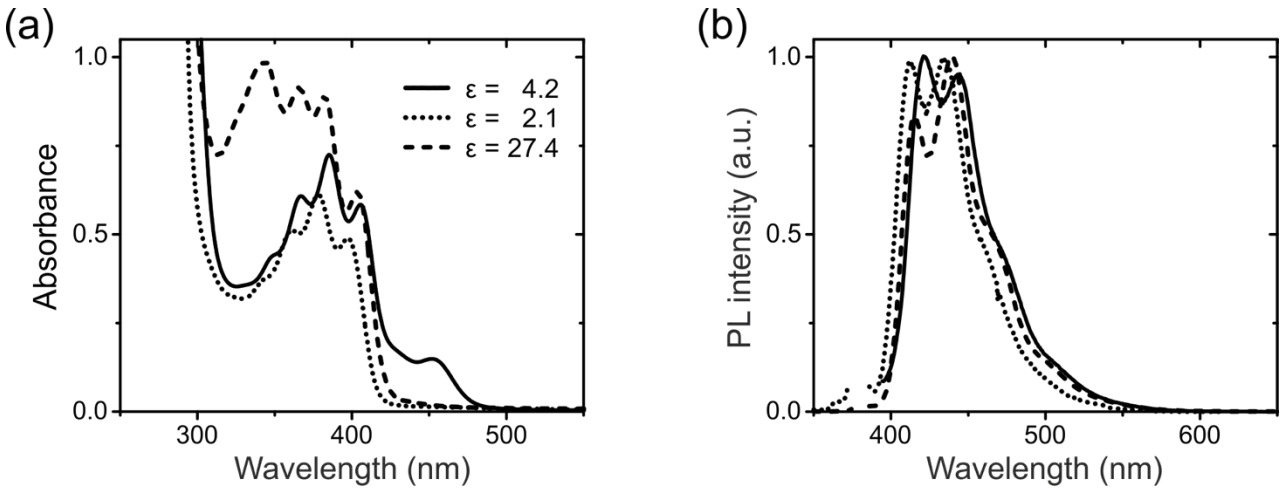

Figure 5. (a) Absorption spectra of PPM (167 mmol L^{-1}, solid line), PMPM (292 mmol L^{-1}, dotted line) and PTMPM (14 mmol L^{-1}, dashed line) in chloroform solutions. The molar extinction coefficients ($\boldsymbol{\varepsilon}$ in L mol^{-1} cm^{-1}) are given in the inset relative to a constitutional repeat unit for λ = 386 nm, λ = 376 nm and λ = 381 nm, respectively. (b) PL spectra of PPM (83 mmol L^{-1}, solid line), PMPM (71 mmol L^{-1}, dotted line) and PTMPM (28 mmol L^{-1}, dashed line) in chloroform solutions recorded with excitation at 388 nm.

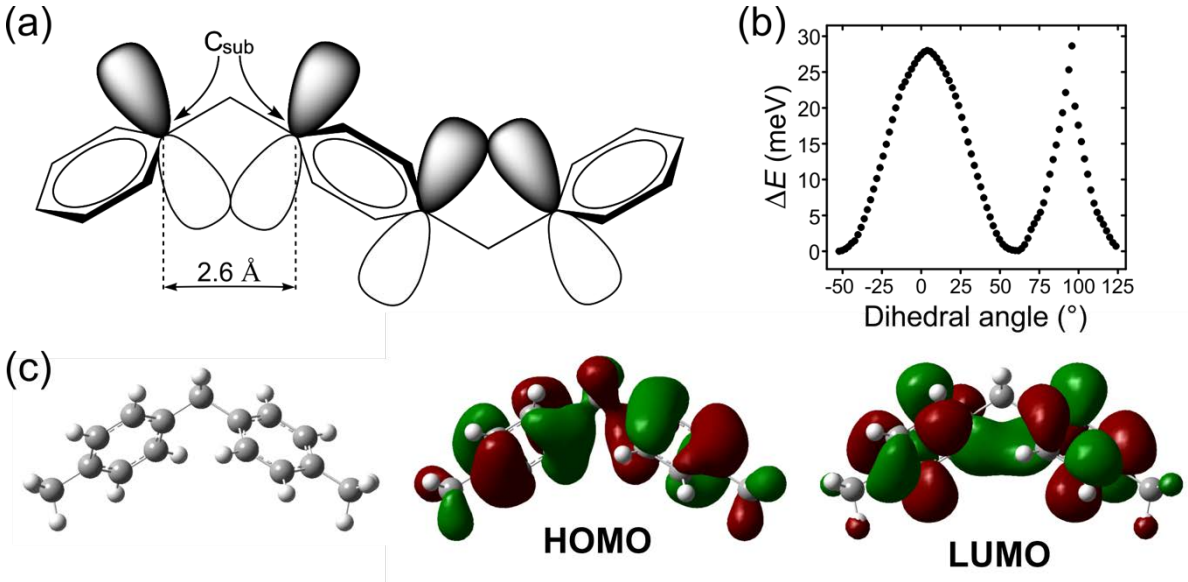

Figure 6. (a) Schematic representation of homoconjugation via π-orbital interaction of C_{sub} atoms in a PPM chain segment featuring a slightly tilted orientation of adjacent phenylene rings. (b) DFT results of relative potential energy $\Delta \boldsymbol{E}$ vs. dihedral angle scan for the para-substituted PPM (quasi) dimer, yielding 56° as the most energetically favorable angle, corresponding to a C_2 point group. (c) Three-dimensional illustration of the lowest energy conformation of a PPM dimer as calculated with DFT, along with iso-surface plots (iso-surface values of $\pm$0.02) of its HOMO and LUMO.

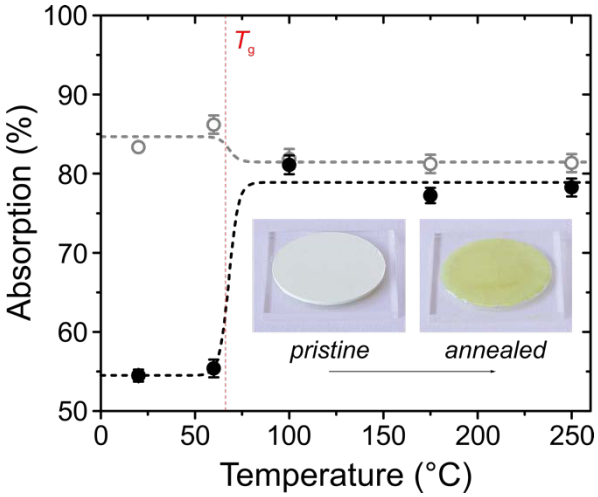

Figure 7. Absorption for a PPM plaque recorded at 280 nm (localized absorption of phenylene; open gray circles) and 366 nm (delocalized S_0-S_1 absorption of the *blue*-phase; solid black circles) after sequential annealing for 5 min at the indicated temperatures (increasing from 20 °C to 250 °C). Inset shows photographs of the *pristine* PPM plaque (diameter of 1.3 cm) prior to annealing and the same plaque *annealed* above the glass transition temperature, T_g (indicated). Dotted black and gray lines serve as a guide for the eye only.

Table 1. Summary of basic structural, thermal and electrochemical properties for the synthesized polymers: number- (M_n) and weight- (M_w) average molar masses; polydispersity indices (PDI = M_w/M_n); glass-transition (T_g) and decomposition (T_{dec}) temperatures; and energy levels of HOMO (E_{HOMO}) and LUMO (E_{LUMO}).

Polymer	M_n [a]	M_w [a]	PDI	T_g [b]	T_{dec} [c]	E_{HOMO} [d]	E_{LUMO} [d]
	[g mol^{-1}]	[g mol^{-1}]		[°C]	[°C]	[eV]	[eV]
PPM	10'900	35'900	3.3	66	470	–5.8	–2.5
PMPM	10'500	52'900	5.0	93	488	–5.8	–2.6
PTMPM	5'000	27'300	6.1	147	450	–5.8	–2.6

Data obtained from: [a] GPC performed at 35 °C in chloroform; [b] DSC on neat polymers; [c] TGA in air (onset temperatures reported); [d] cyclic voltammetry performed in dichloromethane (~30 mmol L^{-1}).

Table 2. Photoluminescence lifetime, τ, measured for PPM thin films (~330 nm), and photoluminescence quantum efficiency (PLQE) determined for PPM films and solutions in chloroform. The respective excitation wavelengths, λ_{ex}, used are indicated.

PPM sample	τ [a]	PLQE [b]
	[ns]	[%]
film	8.55	41 ± 3
solution	–	69 ± 1

[a] λ_{ex} = 379 nm; [b] λ_{ex} = 388 nm (error margins refer to standard deviation)